Electronic Supplementary Information

Synthesis, computational and nanoencapsulation studies on eugenol-derived insecticides

Catarina M. M. Coelho[a], Renato B. Pereira[b], Tatiana F. Vieira[c,d], Cláudia M. Teixeira[a,b], Maria José G. Fernandes[a], Ana Rita O. Rodrigues[e,f], David M. Pereira[b], Sérgio F. Sousa[c,d], A. Gil Fortes[a], Elisabete M. S. Castanheira[e] and M. Sameiro T. Gonçalves[a,*]

[a] *Centre of Chemistry, Department of Chemistry, University of Minho, Campus of Gualtar, 4710-057 Braga, Portugal;*

[b] *REQUIMTE/LAQV, Laboratory of Pharmacognosy, Department of Chemistry, Faculty of Pharmacy, University of Porto, R. Jorge Viterbo Ferreira, 228, 4050-313 Porto, Portugal;*

[c] *UCIBIO/REQUIMTE, BioSIM – Departamento de Medicina, Faculdade de Medicina da Universidade Do Porto, Alameda Prof. Hernâni Monteiro, 4200-319 Porto, Portugal;*

[d] *Associate Laboratory i4HB - Institute for Health and Bioeconomy, Faculdade de Medicina, Universidade do Porto, 4200-319 Porto, Portugal;*

[e] *Physics Centre of Minho and Porto Universities (CF-UM-UP), University of Minho, Campus of Gualtar, 4710-057 Braga, Portugal;*

[f] *Associate Laboratory LaPMET - Laboratory of Physics for Materials and Emergent Technologies, University of Minho, Campus of Gualtar, 4710-057 Braga, Portugal.*

Table S1. Targets selected for the inverted virtual screening assay

Target	Organism	PDB target	Resolu-tion (Å)	Description	Ref
Ecdysone receptor	*Heliothis virescens*	1R20	3.00	VS based on 1R20 bound to an agonist as a model for the development of a receptor-based pharmacophore model.	1
		1R1K	2.90	VS of 2 million compounds against 1R1K, an ecdysone receptor structure bound to its known ligand ponasterone A.	2
Chitinase	*Ostrinia furnacalis*	3WL1	1.77	Pharmacophore-based screening using two crystal structures of chitinases: 3WL1 bound to its reaction product and 3WQV bound to an inhibitor.	3
		3WQV	2.04		
beta-*N*-Acetyl-D-hexosaminidase OfHex1		3NSN	2.10	VS of the ZINC database to identify OfHex1 inhibitors using 3NSN crystal structure bound to a known inhibitor.	4
		3OZP	2.00	VS of the ZINC data-base targeting 3OZP, a crystal structure of OfHex1 bound to an inhibitor.	5
N-Acetylglucosami-ne-1-phosphate uridyltransferase (GlmU)	*Xanthomonas oryzae*	2V0K	2.30	Homology model built for docking using 2V0K and 2VD4 as templates. 2V0K crystal structure is bound to its known ligand and 2VD4 is bound to a possible inhibitor.	6
		2VD4	1.90		
Acetylcholines-terase	*Aedes aegypti*	1QON	2.72	Search for new molecules with insecticidal activity against *Ae. Aegypti* using acetylcholinesterase crystal structures 1QON and 4EY6 as targets, both bound to possible inhibitors.	7
		4EY6	2.40		
	Drosophila melanogaster	1DX4	2.70	Homology 3D model built for VS using 1DX4 as template. 1DX4 crystal structure is bound to a potent inhibitor.	8
Prophenoloxidase (PPO)	*Manduca sexta*	3HSS	1.97	Crystal structure of a prophenoloxidase from *Manduca sexta.*	9
p-Hydroxyphenyl-pyruvate dioxygenase	*Arabidopsis thaliana*	6ISD	2.40	Development of a receptor-ligand pharmacophore model based on the crystal structure 6ISD bound to a commonly used pesticide. The best model created was then used for VS studies.	10
Voltage-gated sodium channel	*Periplaneta americana*	6A95	2.60	Crystallographic structure of a Voltage-gated sodium channel NavPaS bound to a pore blocker, tetrodotoxin (TTX)	11
Octopamine receptor	*Blattella germanica*	4N7C	1.75	Crystal structure of Bla g 4, an octopamine receptor, bound to tyramine.	12
Sterol carrier protein-2 (HaSCP-2)	*Helicoverpa armigera*	4UEI	Solution NMR	Structure-based VS of a database of commercially available compounds to find potential inhibitors of HaSCP-2. The residues Phe53, Thr128, and Gln131 were selected for the binding cavity.	13
Peptide deformylase	*Xanthomonas oryzae*	5CY8	2.38	Docking and VS of a library of 318 phytochemicals. 5CY8 crystal structure is bound to a possible inhibitor.	14
Alpha-esterase-7 (αE7)	*Lucilia cuprina*	5TYJ	1.75	Computational design of potent and selective covalent inhibitors of αE7. 5TYJ and 5TYP crystal structures are bound to inhibitors: (3-bromo-5-phenoxylphenyl)boronic acid and (3-bromo-4-methylphenyl)boronic acid respectively.	15
		5TYP	1.88		
Odorant Binding Protein	*Aedes aegypti*	5V13	1.84	Search for new molecules with insecticidal activity against *Ae. Aegypti* using a crystal structure of a mosquito juvenile hormone-binding protein, 5V13 bound to its natural hormone.	7
	Drosophila melanogaster	2GTE	1.40	2GTE crystal structure is bound to its natural ligand	16
	Anopheles gambiae	3N7H	1.60	QSAR and docking studies for the rational design of mosquito repellents using the crystal structure 3K1E bound to a polyethylene glycol molecule. 3N7H crystal structure is bound to a commonly used repellent.	17
	Aedes aegypti	3K1E	1.85		17

Creation of a homology model

The model generated by SWISS-MODEL for 1QON was used in the MD simulations since the gap that was missing from the original structure was distant from the active site.

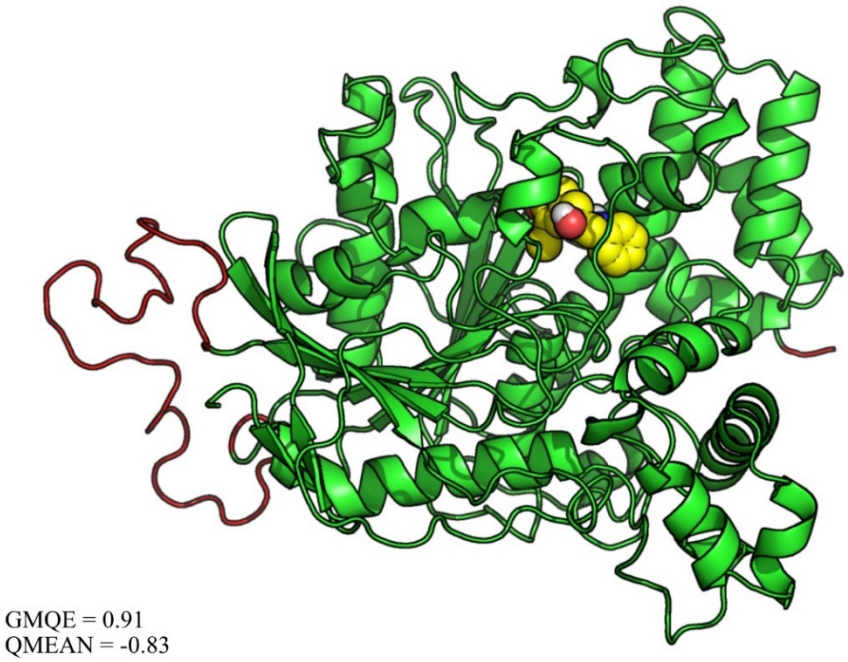

Figure S1. Homology model built for 1QON. Green is the original structure and red represents the loop that was generated by SWISS-MODEL. In yellow is the ligand molecule (**3g**). GMQE - Global Model Quality Estimation, is expressed between 0 and 1 with a higher number meaning higher reliability. QMEAN - provides an estimate of the "degree of nativeness" of the structural features observed in the model. A value of QMEAN around zero indicate a good agreement between the model and experimental structure.

Figure S2. Protein and ligand RMSD (Å) of the AChE and OBP – ligand complexes.

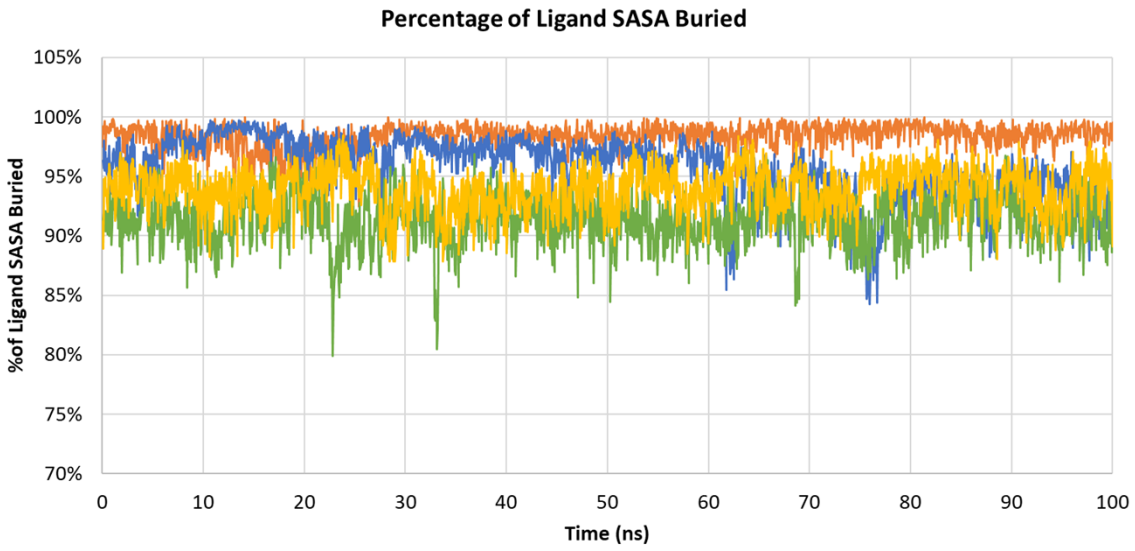

Figure S3. Percentage of the potential solvent accessible surface area of the ligands that is buried by the protein targets evaluated.

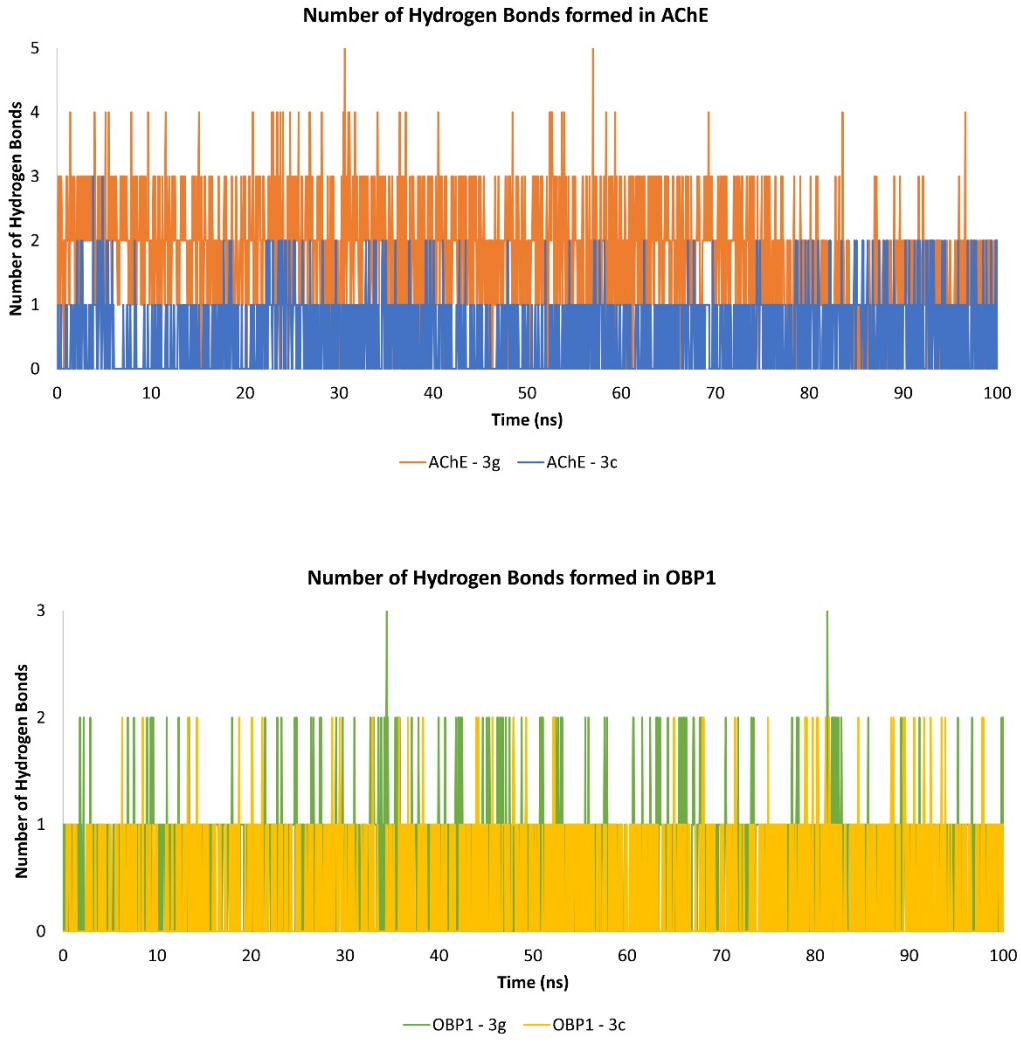

Figure S4. Number of ligand-target hydrogen bonds formed during the simulations for compound **3d** and **3f** when complexed with AchE and OBP.

Table S2. Docking scores for Compound **3c** and **3g** in complex with Human and insect AChE.

		PLP	ASP	ChemScore	GoldScore	Vina
Human AChE	**3c**	69.19	45.37	35.79	55.49	-7.3
Insect AChE	**3c**	72.89	51.12	32.77	59.90	-7.5
Human AChE	**3g**	82.93	54.23	39.29	65.03	-8.5
Insect AChE	**3g**	96.52	60.47	39.41	69.58	-9.0

References

1. Hu X, Yin B, Cappelle K, Swevers L, Smagghe G, Yang X, Zhang L. Identification of novel agonists and antagonists of the ecdysone receptor by virtual screening. *J Mol Graph Model.* 2018;81:77-85. 10.1016/j.jmgm.2018.02.016.

2. Harada T, Nakagawa Y, Ogura T, Yamada Y, Ohe T, Miyagawa H. Virtual screening for ligands of the insect molting hormone receptor. J Chem Inf Model. 2011;51:296-305. 10.1021/ci100400k.

3. Dong Y, Jiang X, Liu T, Ling Y, Yang Q, Zhang L, He X. Structure-Based Virtual Screening, Compound Synthesis, and Bioassay for the Design of Chitinase Inhibitors. *J Agric Food Chem.* 2018;66:3351-3357. 10.1021/acs.jafc.8b00017.

4. Liu J, Liu M, Yao Y, Wang J, Li Y, Li G, Wang Y. Identification of Novel Potential β-N-Acetyl-D-Hexosaminidase Inhibitors by Virtual Screening, Molecular Dynamics Simulation and MM-PBSA Calculations. *Int. J. Mol. Sci.* 2012;13:4545-4563. 10.3390/ijms13044545

5. Dong L, Shen S, Xu Y, Wang L, Yang Q, Zhang J, Lu H. Identification of novel insect β-N-acetylhexosaminidase OfHex1 inhibitors based on virtual screening, biological evaluation, and molecular dynamics simulation. *J Biomol Struct Dyn.* 2021;39:1735-1743. 10.1080/07391102.2020.1743758.

6. Min J, Lin D, Zhang Q, Zhang J, Yu Z. Structure-based virtual screening of novel inhibitors of the uridyltransferase activity of Xanthomonas oryzae pv. oryzae GlmU. *Eur J Med Chem.* 2012;53:150-158. 10.1016/j.ejmech.2012.03.051.

7. Ramos RS, Costa JC, Silva RC, Costa GV, Rodrigues ABL, Rabelo EM, Souto RNP, Taft CA, Silva CHTP, Rosa JMC, Santos CBR, Macêdo WJC. Identification of Potential Inhibitors from Pyriproxyfen with Insecticidal Activity by Virtual Screening. *Pharmaceuticals*. 2019;12, 20. 10.3390/ph12010020

8. Riva C, Suzanne P, Charpentier G, Dulin F, Halm-Lemeille MP, Sopkova-de Oliveira Santos J. In silico chemical library screening and experimental validation of novel compounds with potential varroacide activities. *Pestic Biochem Physiol.* 2019;160:11-19.10. 1016/j.pestbp.2019.05.012.

9. Li Y, Wang Y, Jiang H, Deng J. Crystal structure of Manduca sexta prophenoloxidase provides insights into the mechanism of type 3 copper enzymes. *Proc. Natl. Acad. Sci.* 2009;106:17002-17006. 10.1073pnas.0906095106

10. Fu Y, Liu Y-X, Kang T, Sun Y-N, Li J-Z, Ye F. Identification of novel inhibitors of p-hydroxyphenylpyruvate dioxygenase using receptor-based virtual screening. *J Taiwan Inst Chem Eng.* 2019;103:33-43. 10.3390/ijms21155546

11. Shen H, Li Z, Jiang Y, Pan X, Wu J, Cristofori-Armstrong B, Smith JJ, Chin YKY, Lei J, Zhou Q, King GF, Yan N. Structural basis for the modulation of voltage-gated sodium channels by animal toxins. Science. 2018;362:1-8. 10.1126/science.aau2596

12. Offermann LR, Chan SL, Osinski T, Tan YW, Chew FT, Sivaraman J, Mok Y-K, Minor W, Chruszcz M. The major cockroach allergen Bla g 4 binds tyramine and octopamine. *Mol Immunol.* 2014;60:86-94. 10.1016/j.molimm.2014.03.016

13. Cai J, Du X, Wang C, Lin J, Du X. Identification of Potential Helicoverpa armigera (Lepidoptera: Noctuidae) Sterol Carrier Protein-2 Inhibitors Through High-Throughput Virtual Screening. *J Econ Entomol.* 2017;110(4):1779-1784. 10.1093/jee/tox157.

14. Joshi T, Joshi T, Sharma P, Chandra S, Pande V. Molecular docking and molecular dynamics simulation approach to screen natural compounds for inhibition of *Xanthomonas oryzae pv. Oryzae* by targeting peptide deformylase. J Biomol Struct Dyn. 2021;39:823-840. 10.1080/07391102.2020.1719200

15. Correy GJ, Zaidman D, Harmelin A, Carvalho S, Mabbitt PD, Calaora V, James PJ, Kotze AZ, Jackson CJ, London N. Overcoming insecticide resistance through computational inhibitor design. *Proc. Natl. Acad. Sci*. 2019;116:21012-21021. https://doi.org/10.1073/pnas.1909130116

16. Laughlin JD, Ha TS, Jones DNM, Smith DP. Activation of pheromone-sensitive neurons is mediated by conformational activation of pheromone-binding protein. *Cell.* 2008;133:1255-1265. 10.1016/j.cell.2008.04.046.

17. Oliferenko PV, Oliferenko AA, Poda GP, Osolodkin DI, Pillai GG, Bernier UR, Tsikolia M, Agramonte NM, Clark GG, Linthicum KJ, Katritzky AR. Promising Aedes aegypti Repellent Chemotypes Identified through Integrated QSAR, Virtual Screening, Synthesis, and Bioassay. Oliveira, P.L. Editor, *PLoS One.* 2013;8:e64547. https://doi.org/10.1371/journal.pone.0064547

Calibration curves of fluorescence intensity vs. concentration for compound encapsulation and release assays

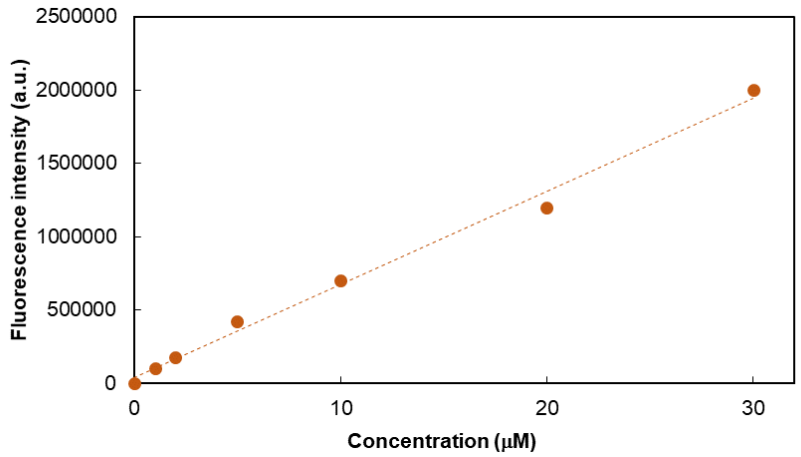

Figure S5. Calibration curve of fluorescence intensity vs. concentration for compound **3c**.

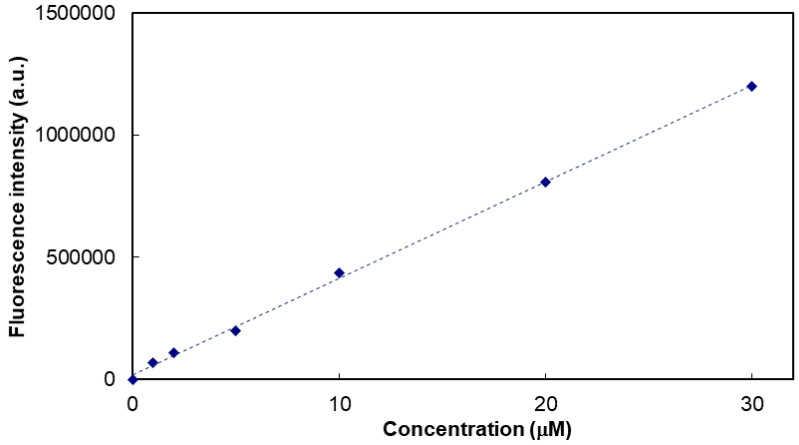

Figure S6. Calibration curve of fluorescence intensity vs. concentration for compound **3g**.

^{1}H and ^{13}C NMR spectra of compounds 3a-g

^{1}H NMR spectra of compounds **3a-g** are shown. These spectra confirm the corresponding structure and purity of each compound. In addition, ^{13}C spectra are also shown. This information serves as the statement for confirming the purity (≥ 95%) of the compounds synthesized in the reported work.

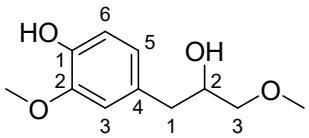
HO
OH
O
O
1
2
3
4
5
6
1
2
3

3a

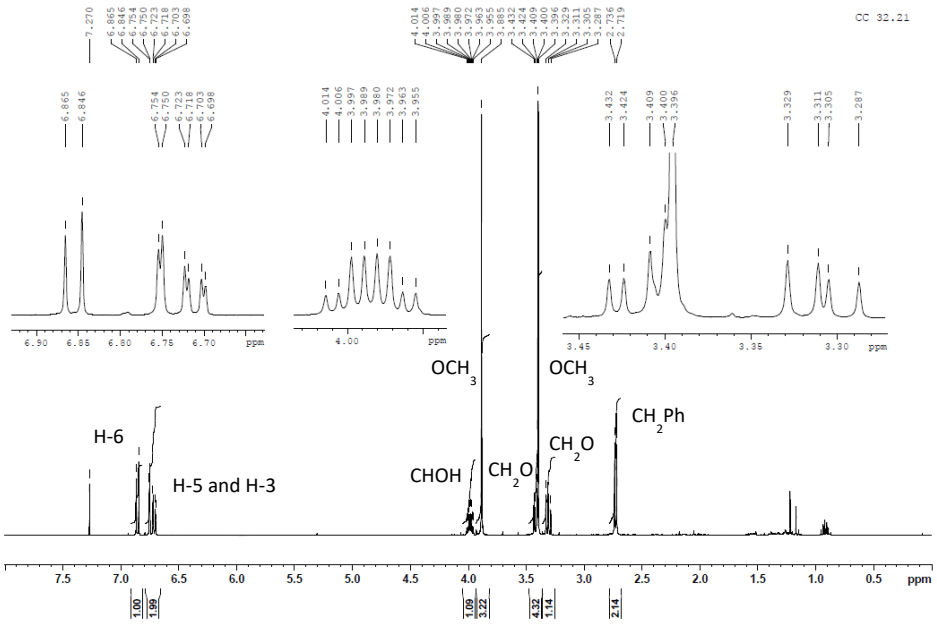
CC 32.21
H-6
H-5 and H-3
CHOH
OCH3
CH2O
OCH3
CH2O
CH2Ph
ppm

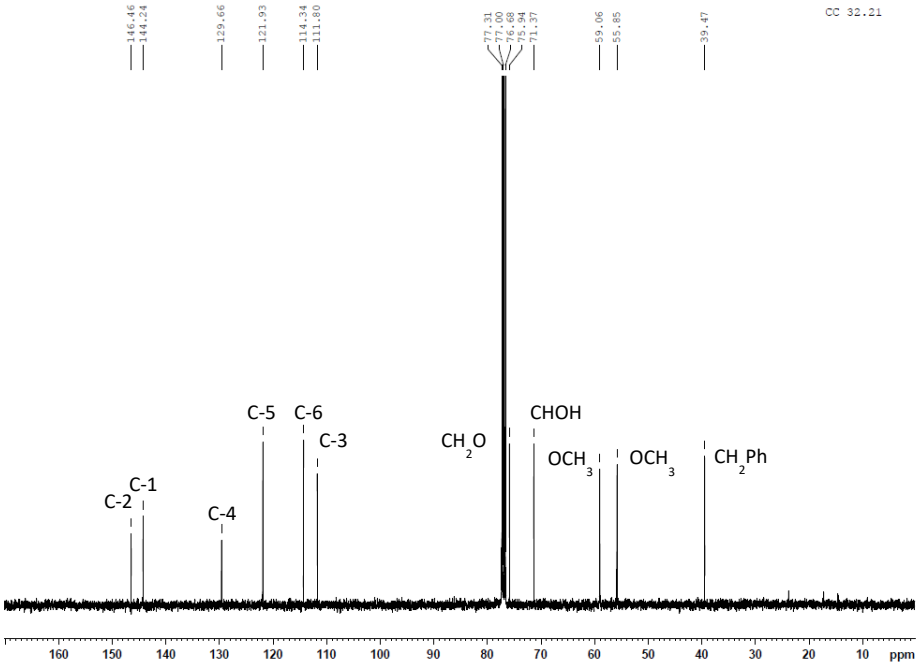
CC 32.21
C-2
C-1
C-4
C-5
C-6
C-3
CH2O
CHOH
OCH3
OCH3
CH2Ph
ppm

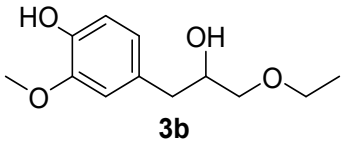
HO
OH
O
O

3b

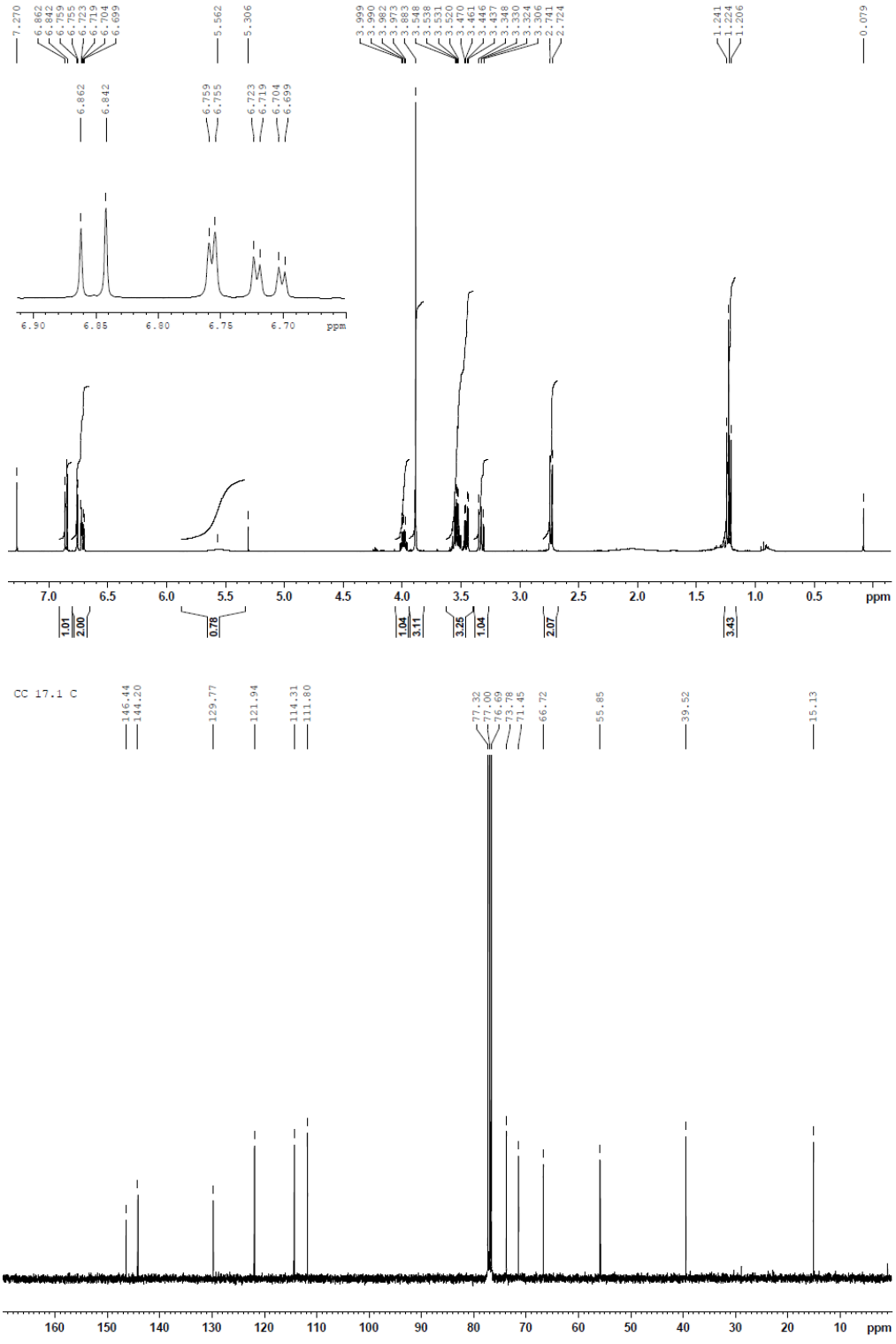
7.270
6.862
6.842
6.759
6.755
6.723
6.719
6.704
6.699
5.562
5.306
3.999
3.990
3.982
3.973
3.883
3.548
3.538
3.531
3.520
3.470
3.461
3.446
3.437
3.348
3.330
3.324
3.306
2.741
2.724
1.241
1.224
1.206
0.079
6.90
6.85
6.80
6.75
6.70
ppm
7.0
6.5
6.0
5.5
5.0
4.5
4.0
3.5
3.0
2.5
2.0
1.5
1.0
0.5
ppm
1.01
2.00
0.70
1.04
3.11
3.25
1.04
2.07
3.43
CC 17.1 C
146.44
144.20
129.77
121.94
114.31
111.80
77.32
77.00
76.68
73.78
71.45
66.72
55.85
39.52
15.13
160
150
140
130
120
110
100
90
80
70
60
50
40
30
20
10
ppm

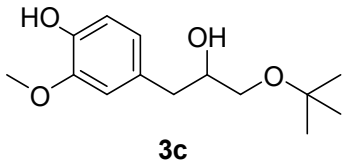
HO
OH
O
O

3c

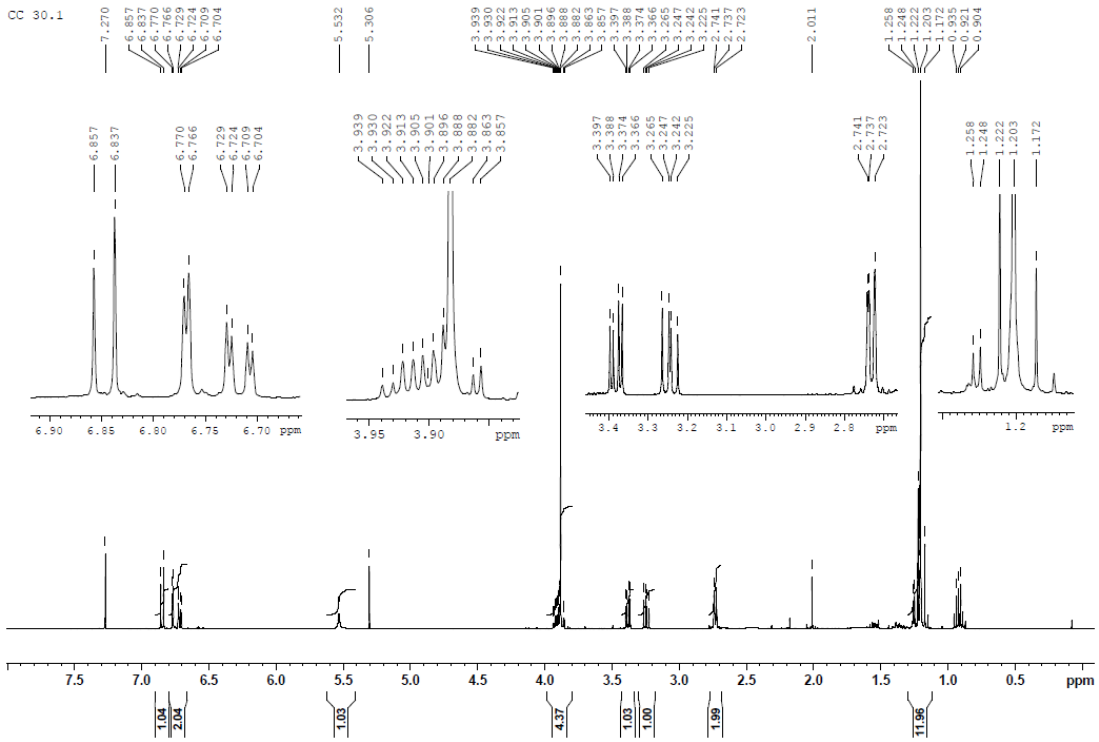
CC 30.1
7.270
6.857
6.837
6.770
6.766
6.729
6.724
6.709
6.704
5.532
5.306
3.939
3.930
3.922
3.913
3.905
3.901
3.896
3.888
3.882
3.863
3.857
3.397
3.388
3.374
3.366
3.265
3.247
3.242
3.225
2.741
2.737
2.723
2.011
1.258
1.248
1.222
1.203
1.172
0.935
0.921
0.904
ppm
1.04
2.04
1.03
4.37
1.03
1.00
1.99
11.96

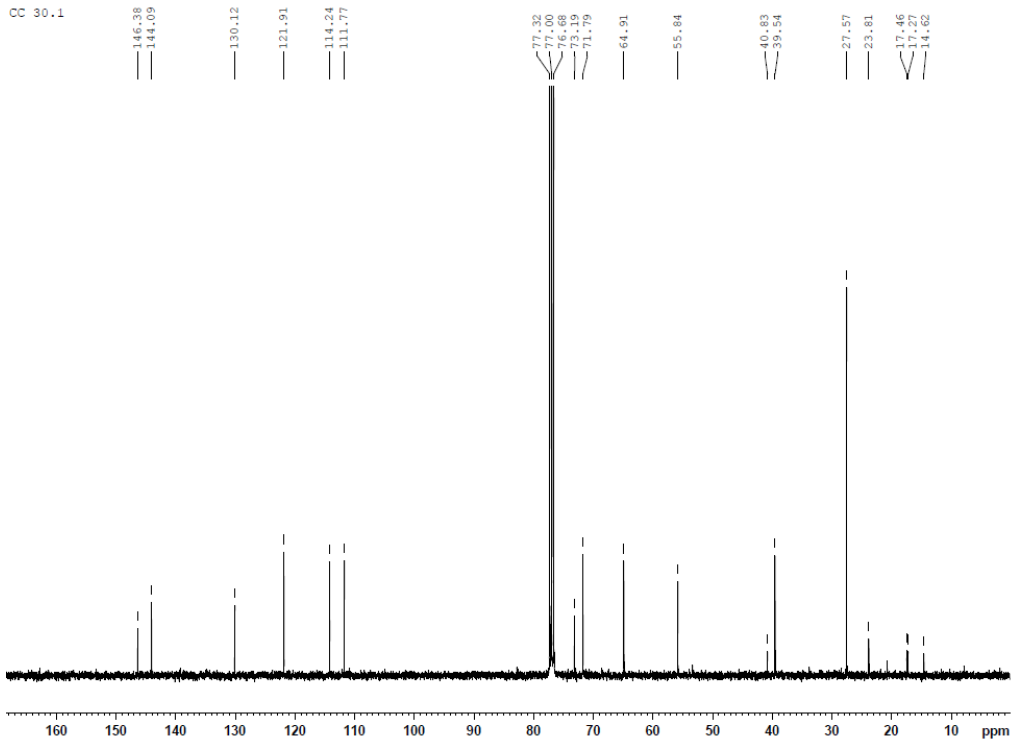
CC 30.1
146.38
144.09
130.12
121.91
114.24
111.77
77.32
77.00
76.68
73.39
71.79
64.91
55.84
40.83
39.54
27.57
23.81
17.46
17.27
14.62
ppm

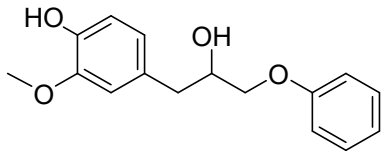

3d

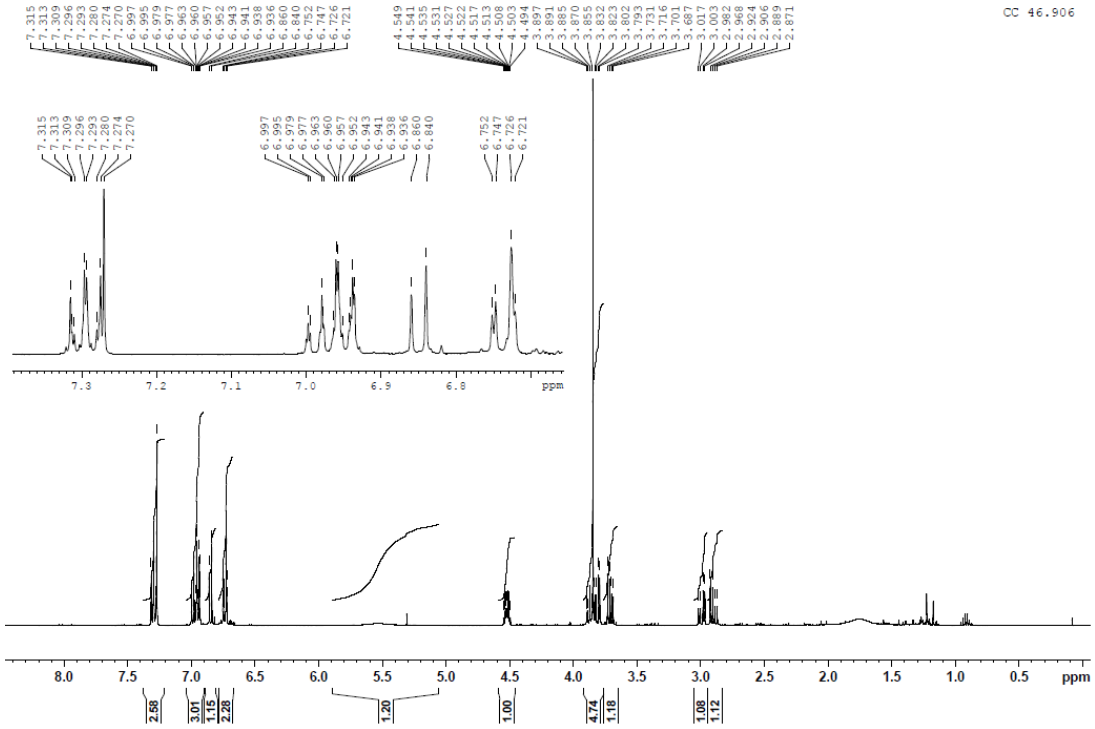

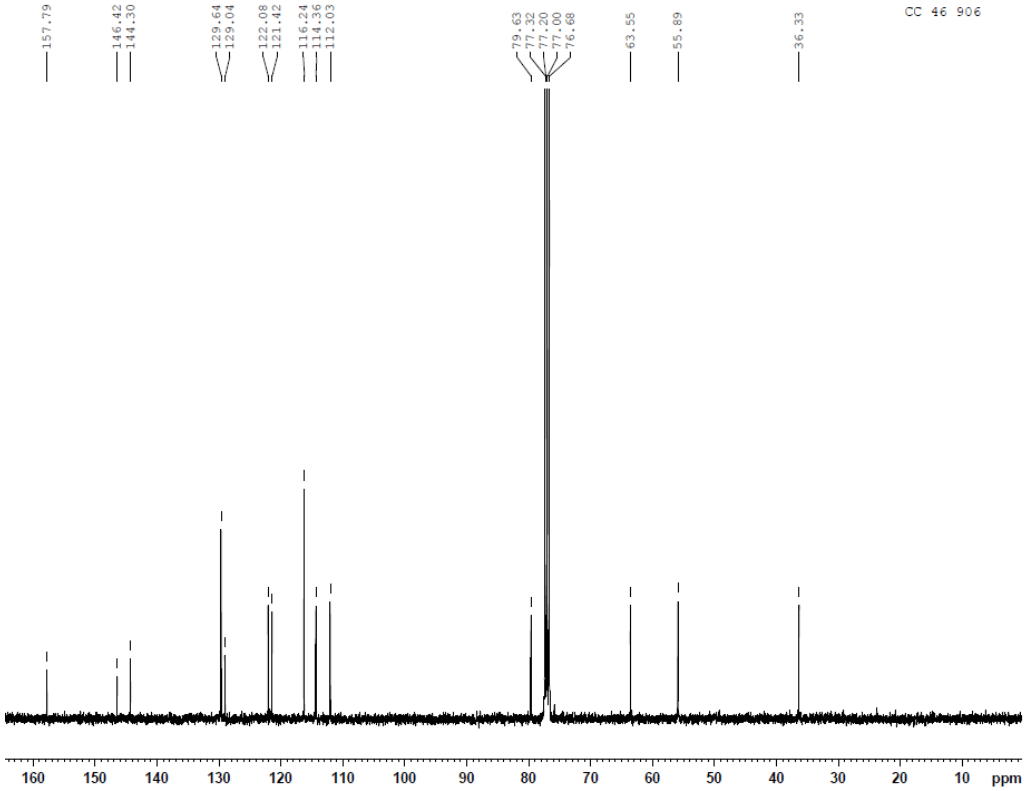

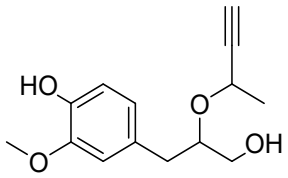
HO
O
O
OH

3e

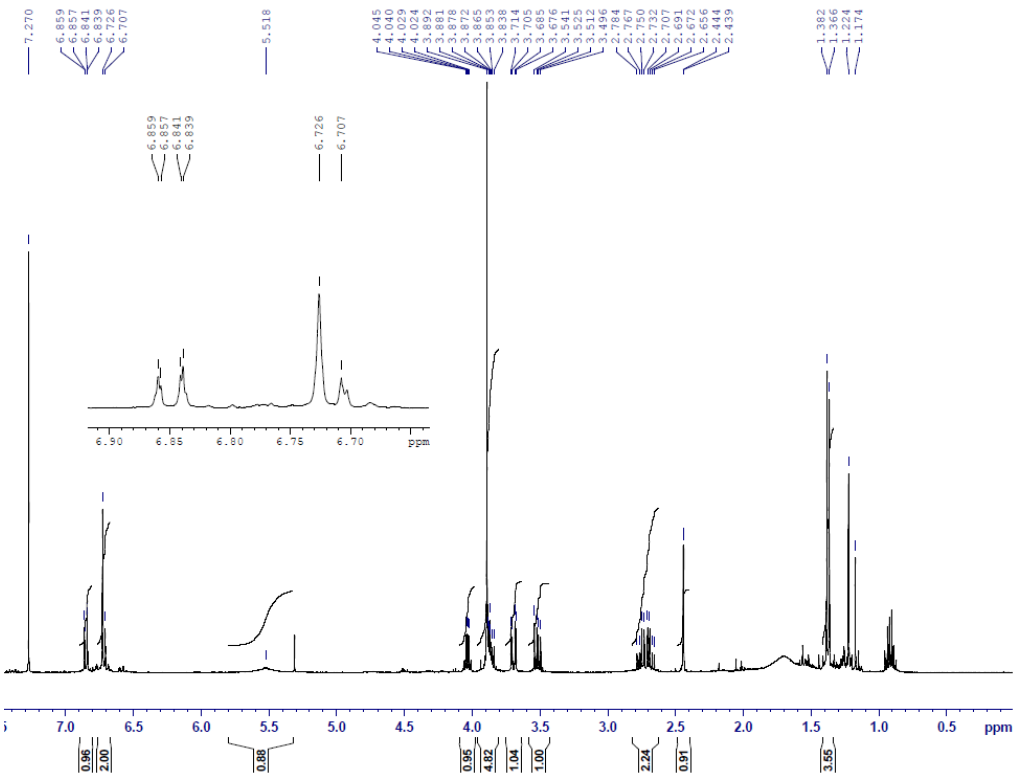
7.270
6.859
6.857
6.841
6.839
6.726
6.707
5.518
4.045
4.040
4.029
4.024
3.892
3.881
3.878
3.872
3.865
3.853
3.838
3.714
3.705
3.685
3.676
3.541
3.525
3.512
3.496
2.784
2.767
2.750
2.732
2.707
2.691
2.672
2.656
2.444
2.439
1.382
1.366
1.224
1.174
ppm
0.96
2.00
0.88
0.95
4.02
1.04
1.00
2.24
0.91
3.65

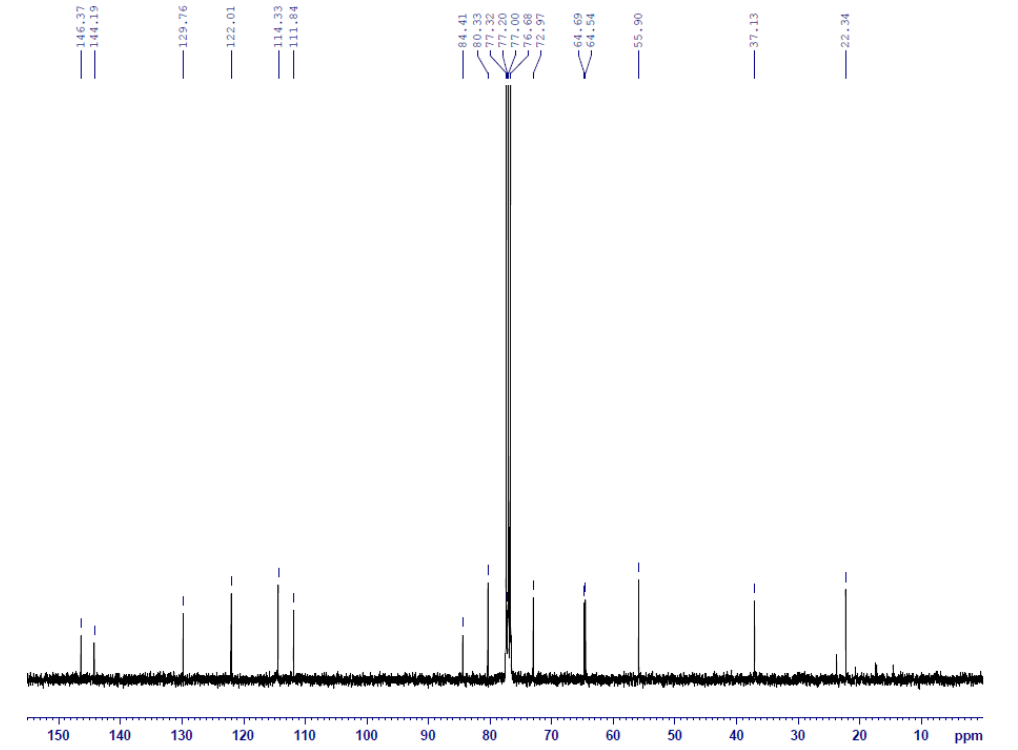
146.37
144.19
129.76
122.01
114.33
111.84
84.41
80.33
77.32
77.20
77.00
76.68
72.97
64.69
64.54
55.90
37.13
22.34
ppm

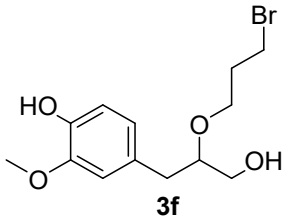

3f

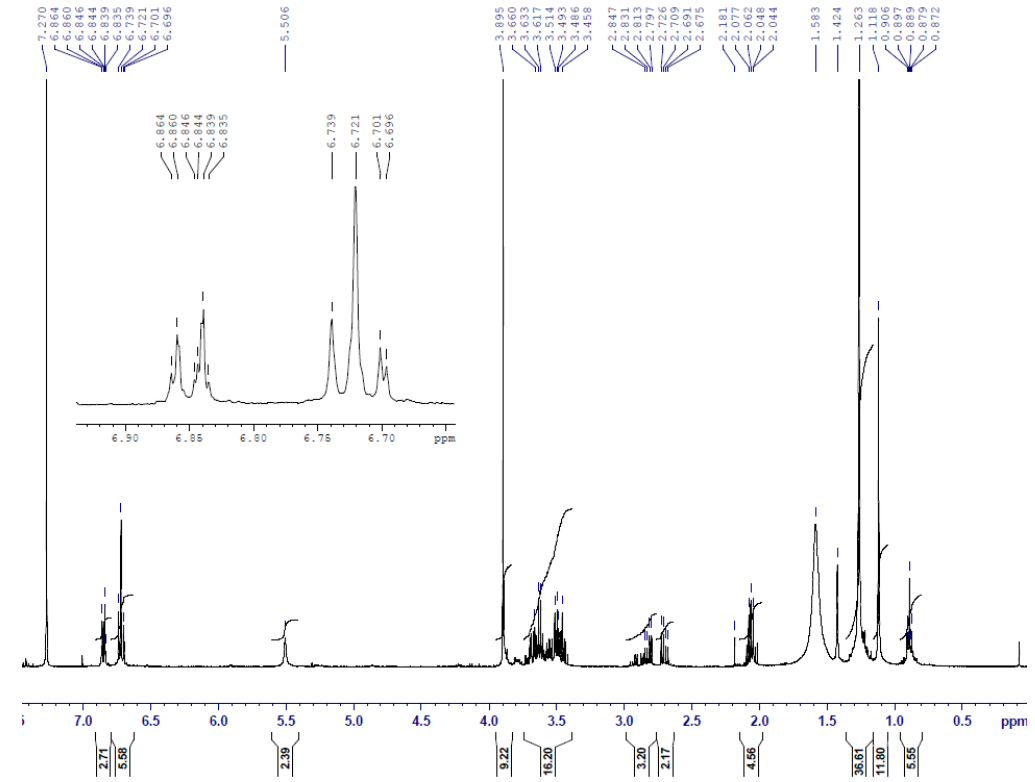

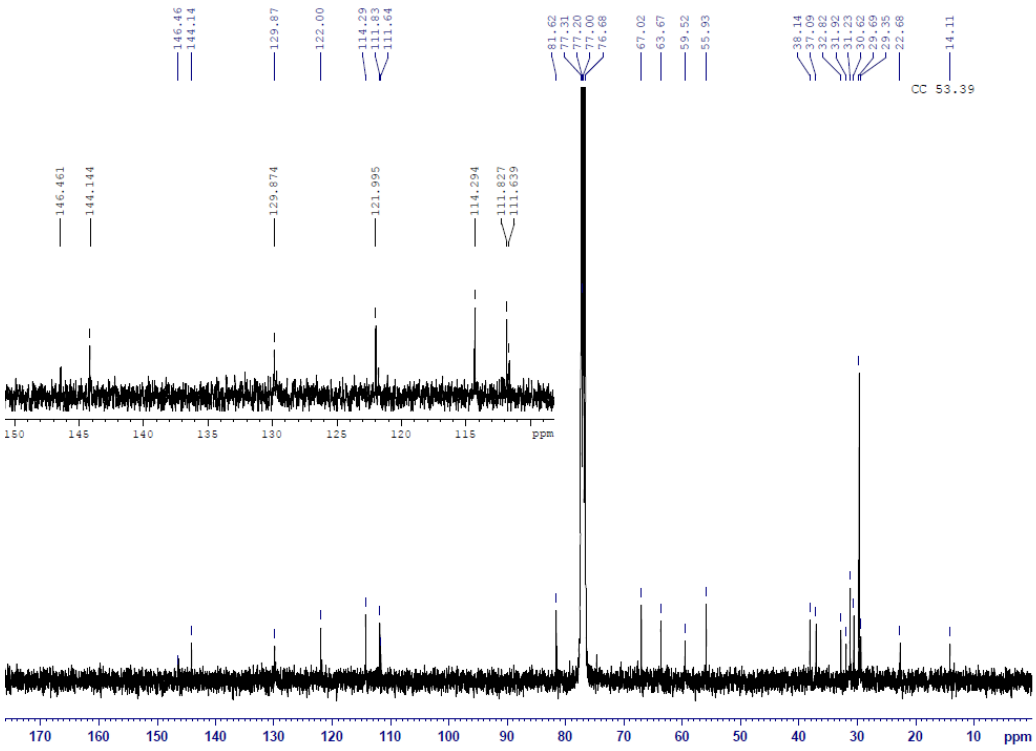

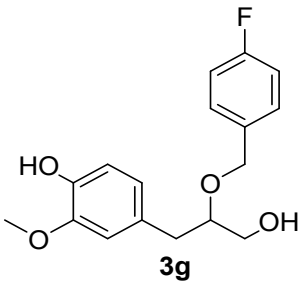
F
HO
O
OH
O

3g

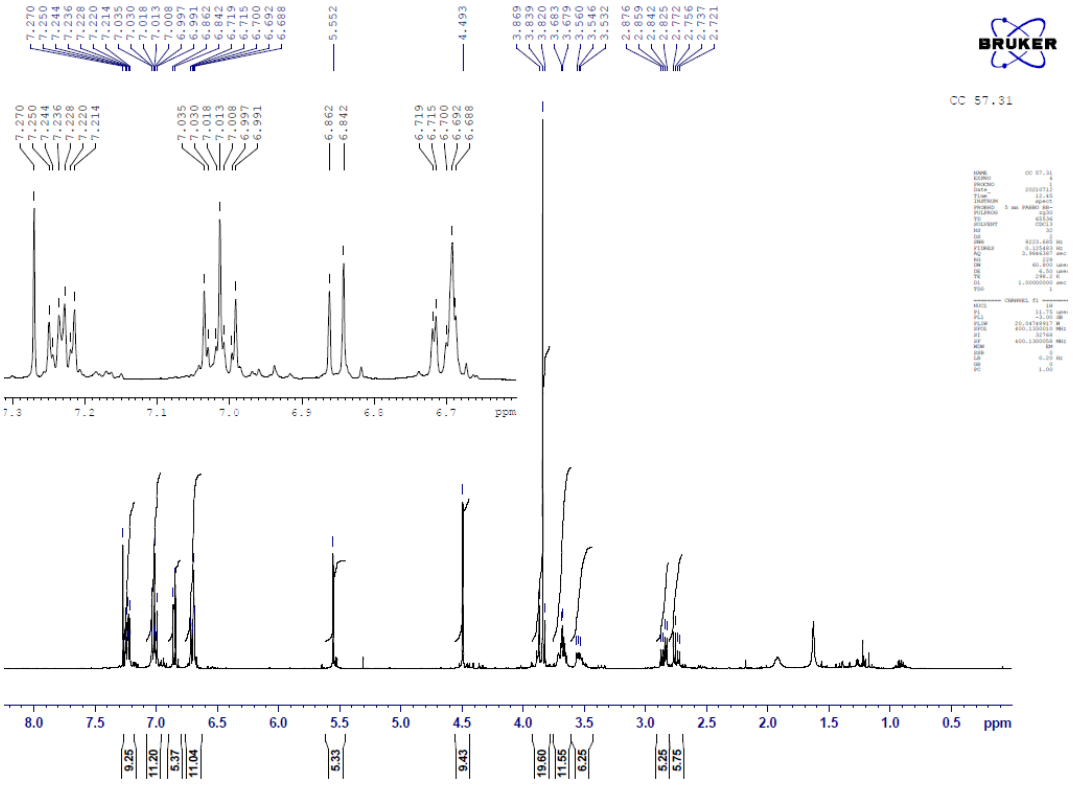
7.270
7.250
7.244
7.236
7.228
7.220
7.214
7.035
7.030
7.018
7.013
7.008
6.997
6.991
6.862
6.842
6.719
6.715
6.700
6.692
6.688
5.552
4.493
3.869
3.839
3.820
3.683
3.679
3.560
3.546
3.532
2.876
2.855
2.842
2.825
2.772
2.756
2.737
2.721
BRUKER
CC 57.31
8.0
7.5
7.0
6.5
6.0
5.5
5.0
4.5
4.0
3.5
3.0
2.5
2.0
1.5
1.0
0.5
ppm
9.25
11.20
5.37
11.04
5.33
9.43
19.60
11.55
6.25
5.25
5.75

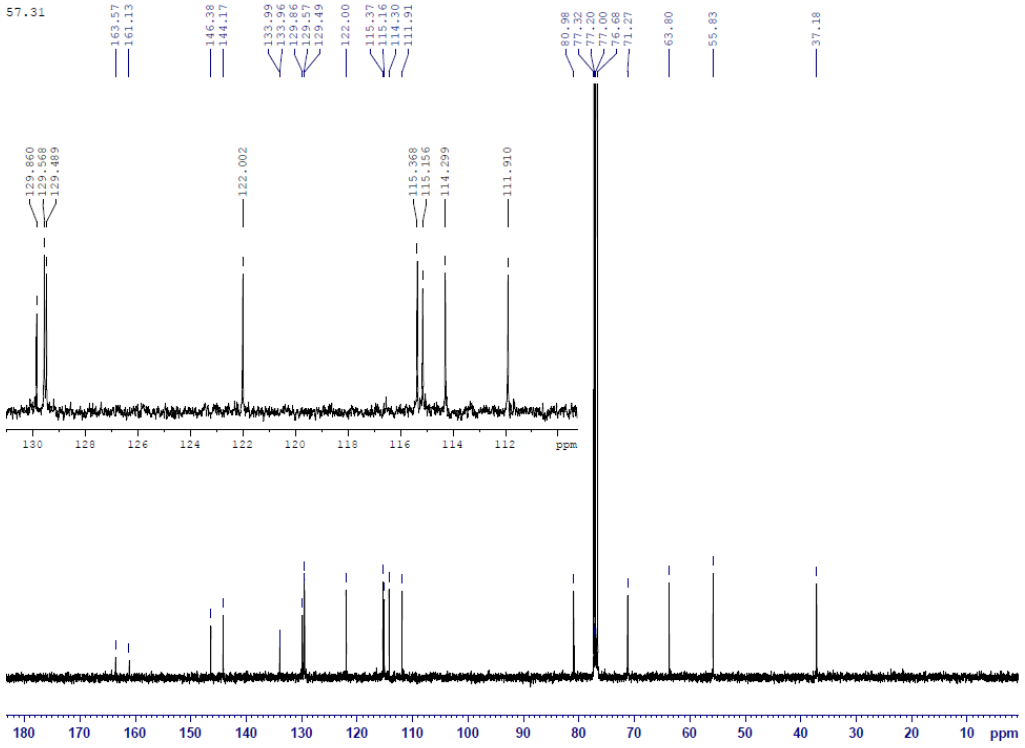
57.31
163.57
161.13
146.38
144.17
133.99
133.96
129.86
129.57
129.49
122.00
115.37
115.16
114.30
111.91
80.98
77.32
77.20
77.00
76.68
71.27
63.80
55.83
37.18
129.860
129.568
129.489
122.002
115.368
115.156
114.299
111.910
130
128
126
124
122
120
118
116
114
112
ppm
180
170
160
150
140
130
120
110
100
90
80
70
60
50
40
30
20
10
ppm

IR spectra of compounds 3a-g

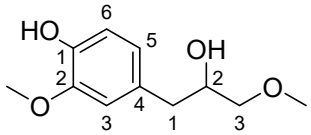

3a

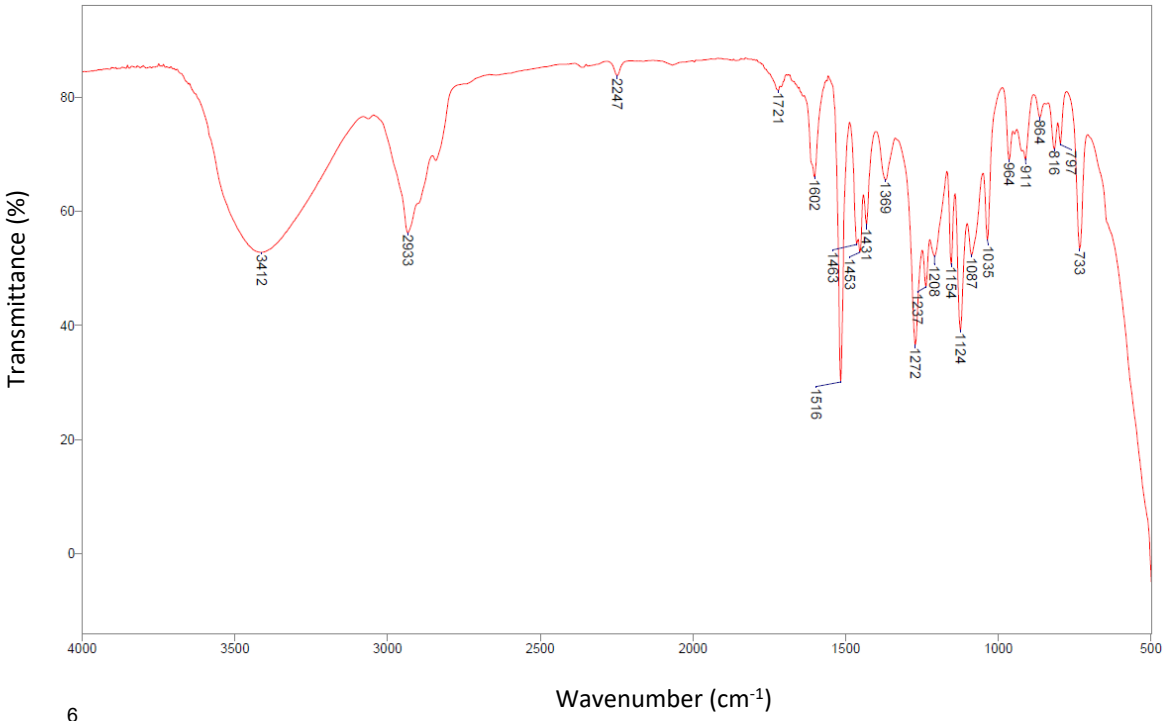

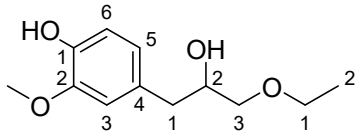

3b

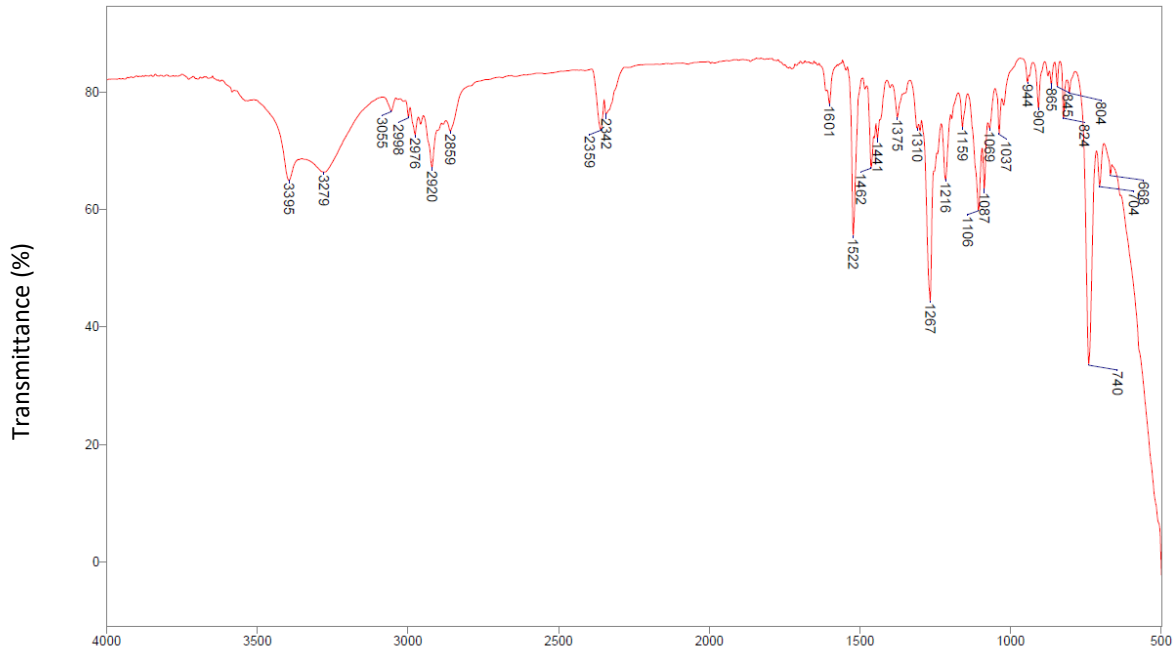

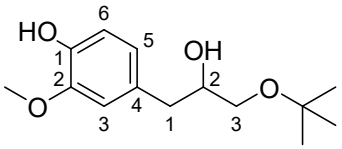
HO
OH
O
O
1
2
3
4
5
6
1
2
3

3c

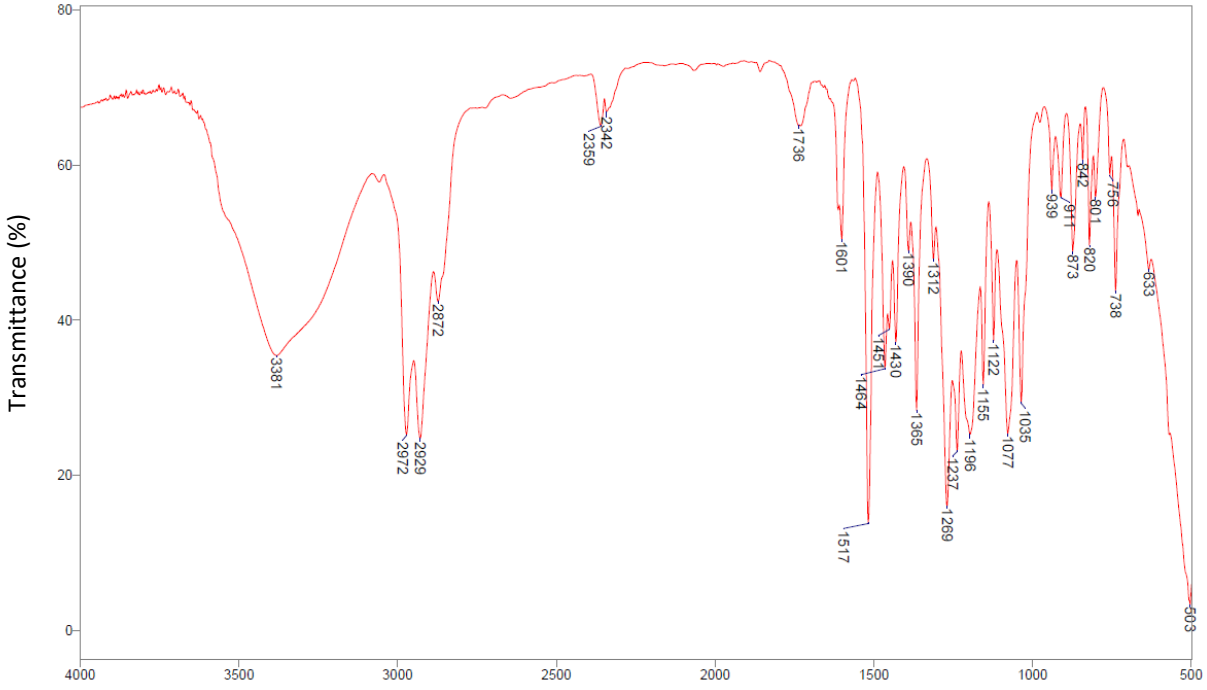
Transmittance (%)
Wavenumber (cm-1)
3381
2972
2929
2872
2359
2342
1736
1601
1517
1464
1451
1430
1390
1365
1312
1289
1237
1196
1155
1122
1077
1035
939
911
873
842
820
801
756
738
633
503

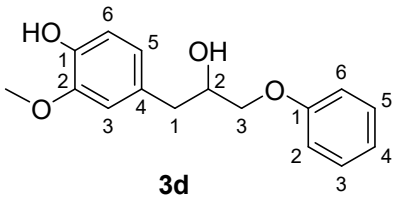
HO
OH
O
O
1
2
3
4
5
6
1
2
3

3d

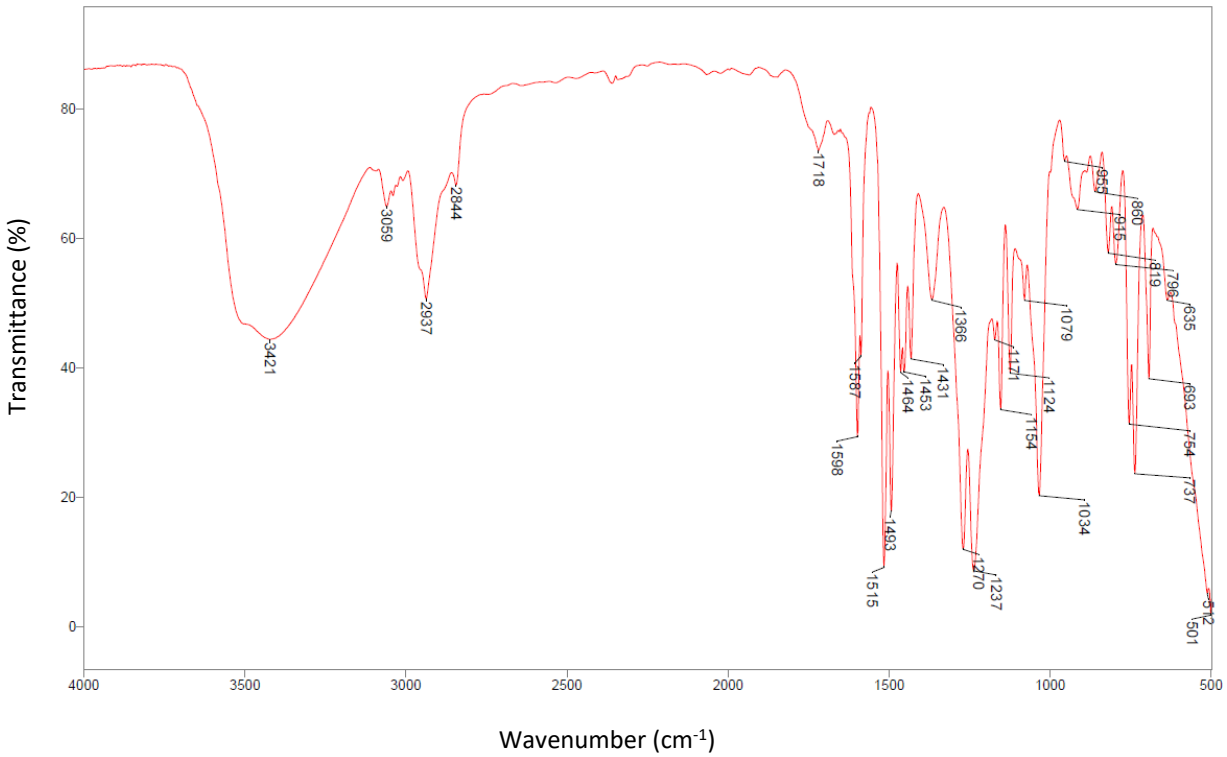
Transmittance (%)
Wavenumber (cm-1)
3421
3059
2937
2844
1718
1598
1587
1515
1493
1464
1453
1431
1366
1270
1237
1154
1124
1079
1034
959
915
860
819
796
737
693
635
754
612
501

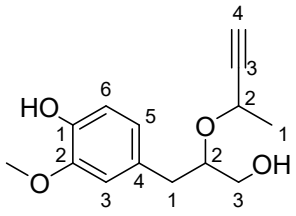
HO
O
OH
O
1
2
3
4
5
6

3e

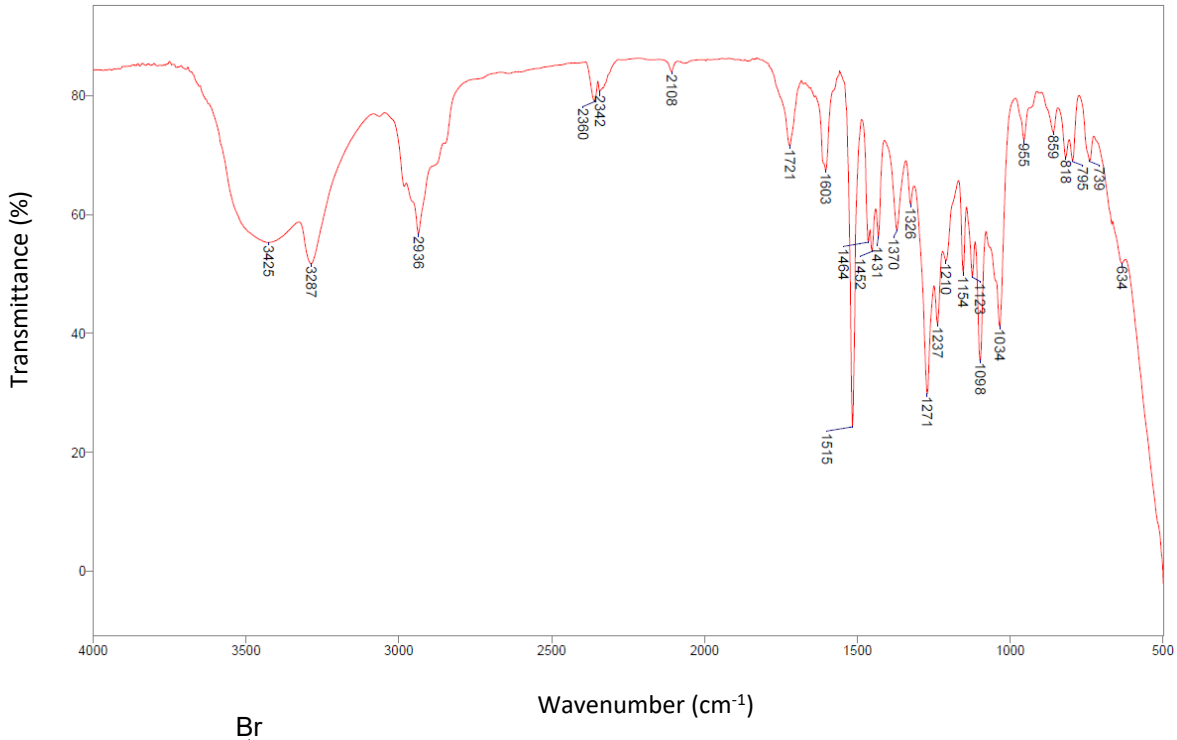
Transmittance (%)
Wavenumber (cm-1)
3425
3287
2936
2360
2342
2108
1721
1603
1515
1464
1452
1431
1370
1326
1271
1237
1210
1154
1123
1098
1034
955
859
818
795
739
634
4000
3500
3000
2500
2000
1500
1000
500
0
20
40
60
80

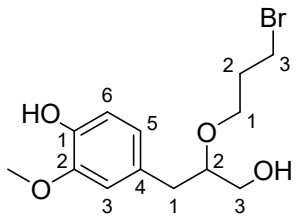
Br
HO
O
OH
O
1
2
3
4
5
6

3f

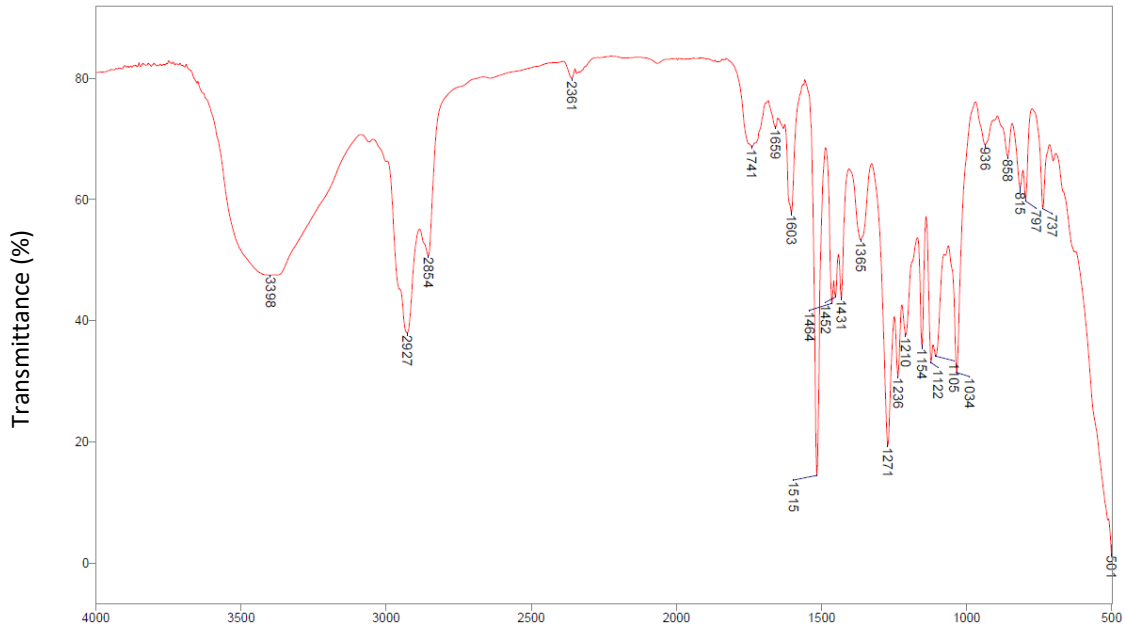
Transmittance (%)
Wavenumber (cm-1)
3398
2927
2854
2361
1741
1659
1603
1515
1464
1452
1431
1365
1271
1236
1210
1154
1122
1105
1034
936
858
815
797
737
501
4000
3500
3000
2500
2000
1500
1000
500
0
20
40
60
80

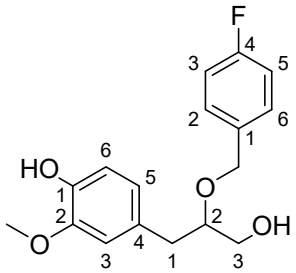
F
HO
O
OH
O

3g

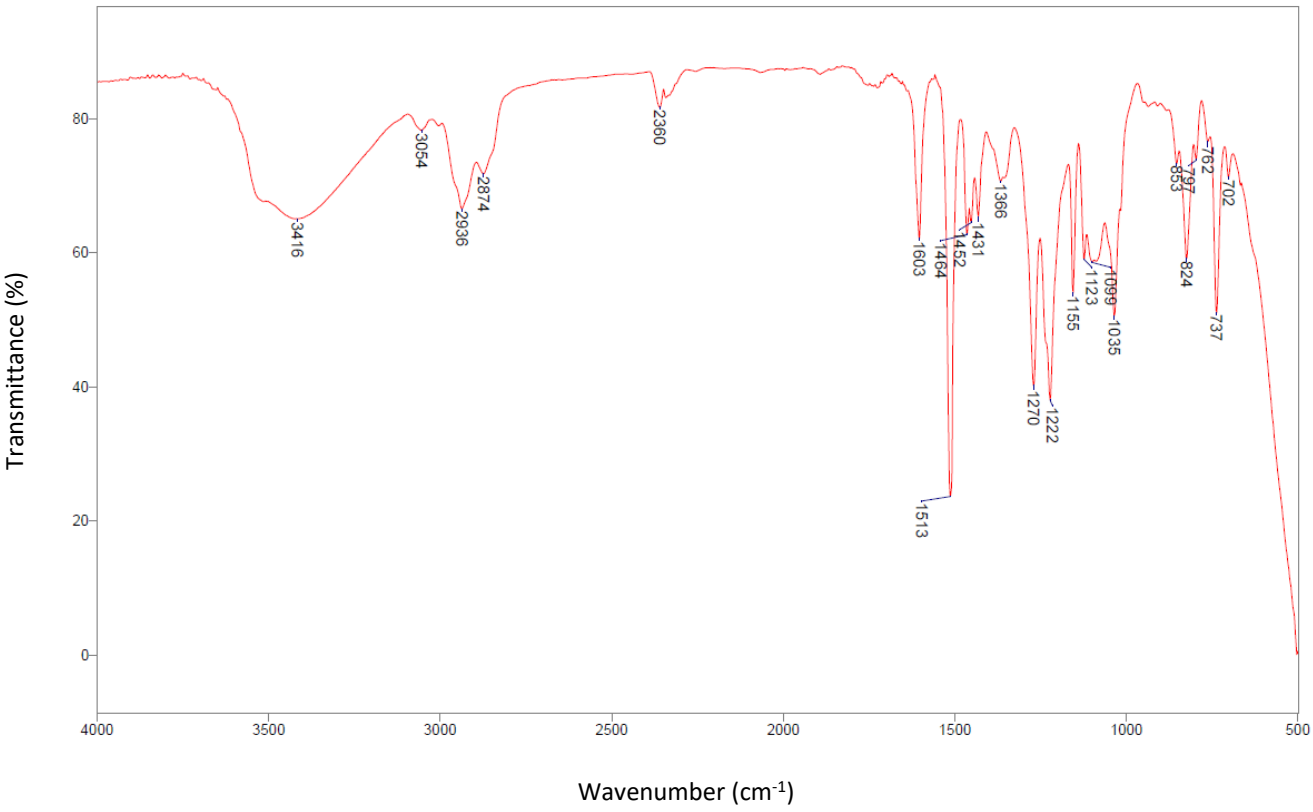
Transmittance (%)
Wavenumber (cm-1)
3416
3054
2936
2874
2360
1603
1513
1464
1452
1431
1366
1270
1222
1155
1123
1099
1035
853
824
797
762
737
702